JOURNAL OF MATERIAL SCIENCE 27 (1992) 777–785.

Measurement of the anisotropic strength and toughness of Pitch-55 carbon ribbons

V. GUPTA*, A. S. ARGON
Massachusetts Institute of Technology, Cambridge, MA 02139, USA

Composites with long reinforcing fibres can be effectively toughened by controlled crack deflection at interfaces of such reinforcements. An important element in achieving this end is the measurement of the strength and toughness of the reinforcing fibres. Here we present results of such experiments. Since measurements of these properties are difficult in fibres of micron dimensions, specially prepared Pitch-55 ribbons of 600 μm width and 35 μm thickness were obtained for doing the tests. As with carbon fibres, these ribbons show strong anisotropy in their elastic and inelastic properties. Hence, the work of fracture along and across the graphitic planes were determined. The average longitudinal tensile strength of these ribbons was found to be 0.6 GPa. Due to inhomogeneities and a possible associated size effect this value is considerably lower for ribbons than that for fibres. The average specific work of fracture of the ribbons across the graphitic planes was determined to be 3.5 $J m^{-2}$. Unusually high values of works of fracture of 166 $J m^{-2}$ were obtained for cracks propagating along the longitudinal graphitic lamellae. These high values were attributed to a profuse kinking type of plasticity on the graphitic lamellae lying parallel to the crack plane. An asymptotic elastic-plastic analysis for single crystals due to Rice [12], was used to estimate the level of inelastic energy dissipation. These estimates were close to the experimentally observed values. The calculation of the dissipated inelastic energy requires knowledge of the interlaminar shear strength across the graphitic lamellae. A torsion experiment was designed to measure the interlaminar shear strength across the weak graphitic planes, giving a value of 83 MPa. An in-plane longitudinal shear modulus of 65 GPa was obtained from the linear portion of the quasi-static torque twist curve of the ribbon. Another measure of this modulus was determined independently from torsional vibration tests, giving an average value of 51 GPa.

1. Introduction

In many aligned fibre reinforced composites, the structural service requirements are almost entirely met by the volume fraction of stiff and strong, but brittle fibres. The matrix then acts merely to position the fibres in space and to impart to the composite a minimum level of transverse tensile and longitudinal shear properties. It is now well recognized, however, that in such composites, the evolution of subcritical damage under stress by correlated fibre fractures is governed by the mechanical coupling of the fibres by the matrix. When the interface transmits all tractions fully, and the coupling between the fibres is too good, isolated fractures in fibres with small variability in strength tend to spread more readily to surrounding fibres, and hasten the development of a super-critical damage cluster (e.g., Argon [1, 2]). In such instances, the strength of the composite is often less than the average strength of an unbonded bundle of similar fibres of equal length [2]. These composites can be made more damage tolerant, by decoupling fractured fibres from their neighbours through controlled delamination along their interfaces. Since most reinforcing fibres are provided with protective coatings, it becomes possible to tailor the strength and toughness of the interfaces between the coating and the fibre in order to decouple the fibre at the interface [3]. The details of the mechanical requirements for decoupling the fibre from impinging cracks at the interface have been discussed elsewhere [1, 4, 5]. Effective use of these criteria require experimental determination of the strength and toughness of the interface between the fibre and its protective coating. In addition, as discussed by Gupta *et al.* [4], the properties of the reinforcing element are also important in achieving high longitudinal toughness and transverse strength of composites. Thus, it is necessary to determine the strength and toughness of the reinforcing elements themselves or of other model materials with analogous micro-structure.

In this communication we discuss the experimental techniques that have been developed to obtain these properties. The reinforcement of interest in the present study is the Pitch-55 carbon fibre. Fibres provided

* *Present address*: Thayer School of Engineering, Dartmouth College, Hanover, NH 03755.

0022–2461/92 $03.00 + .12

with thin protective coatings of SiC are widely used as reinforcing elements in aluminium matrices. Since the experiments are difficult to perform directly on 10 μm diameter fibres, specially prepared ribbons from Pitch-55 material of 600 μm width and 35 μm thickness were obtained for this purpose.*

2. Structure of Pitch-55 carbon ribbons

The Pitch-55 carbon ribbon was prepared using similar polymer precursors as used for the Pitch-55 fibre [6]. Fig. 1a shows a scanning electron micrograph (SEM) of the broad face of a carbon ribbon that is expected to have high strength along its graphitic lamellae and low interlaminar shear strength across them. Furthermore, because of a possible size effect, its axial tensile strength and longitudinal modulus were expected to be somewhat lower than that of the corresponding properties of the fibre. As can be seen in Fig. 1a a certain density of inhomogeneities are present in the ribbon which were expected to result in some strength reduction. Fig. 1b shows a higher magnification view of such an inhomogeneity. These seem to result during the pyrolysing process. Fig. 2a and b give comparative views of the microstructures of a Pitch-55 fibre and the present ribbon as viewed on fracture surfaces. The microstructure of both the fibre and the ribbon have corrugated lamellae aligned along the axial direction. Fig. 3 shows a micrograph of the ribbon cut transversely by a razor blade. The cutting has produced wrinkling of the graphitic lamellae. This suggests the possibility of a low interlaminar shear strength across these graphitic lamellae.

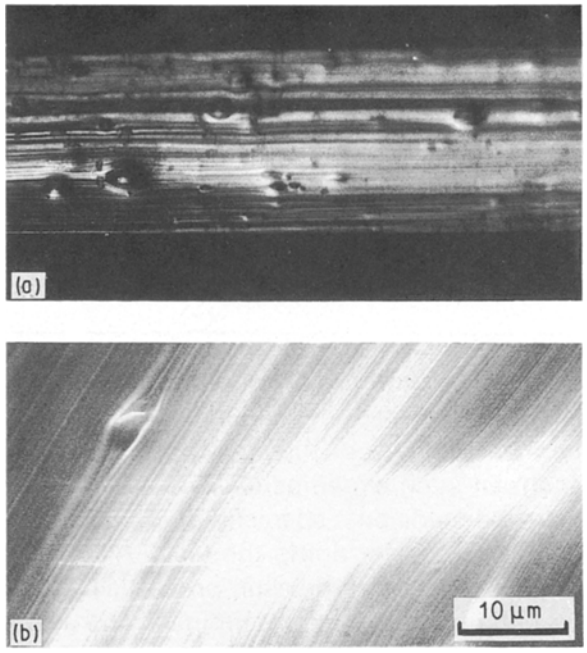

Figure 1 (a) Low magnification micrograph of the carbon ribbon showing structure inhomogeneities, (b) high magnification view of a typical inhomogeneity.

3. Measurement of anisotropic strength of ribbons

3.1. Measurement of strength across the ribbon axis

3.1.1. Specimen preparation and experimental procedure

Tensile strengths of ribbons were determined using a relatively standard procedure. The ribbons were cut into 3.75 cm lengths and mounted individually on rectangular cardboard test frames. The top and bottom of the frames were provided with two punched holes for attachment to the testing machine. The ribbon specimen was centered on the test card to provide a specimen of a gauge length of 2.5 cm. The ends of the ribbon were glued to the card by a Permabond 910 glue.

To perform a test, the intact rectangular cardboard frames each bearing a ribbon specimen were attached to guided pull rods with corresponding pins onto which two punched ends of the cardboard frames could be attached. Once cardboard test frames were fully secured into position, the opposing edges of the test frame, parallel to the ribbon, were cut, permitting the direct loading of the ribbon.

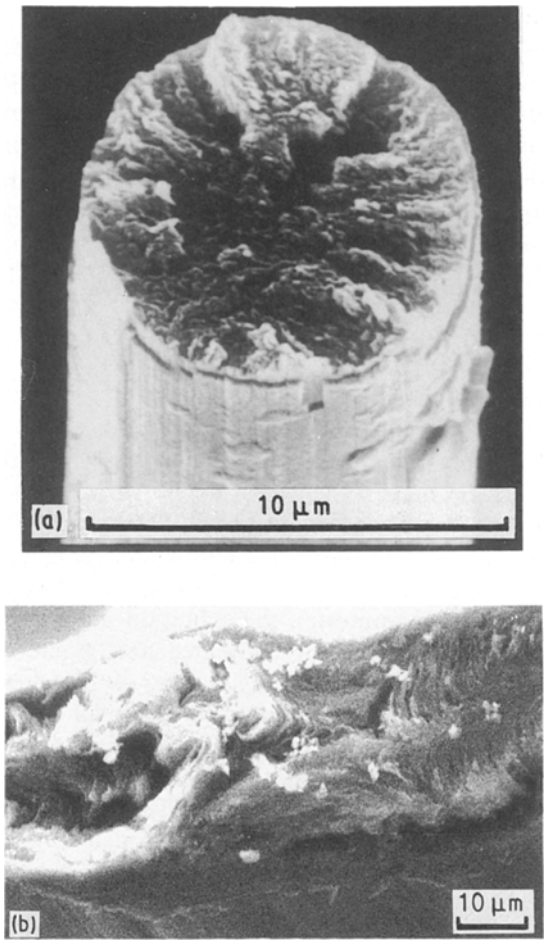

Figure 2 Comparison of the fracture surface morphologies of (a) a Pitch-55 fibre and, (b) the ribbon.

*These exploratory Pitch-55 type carbon ribbons were specially prepared and supplied to us by the Textile Fibers Department of the DuPont Company. For this we are grateful to Dr. E. M. Schultz.

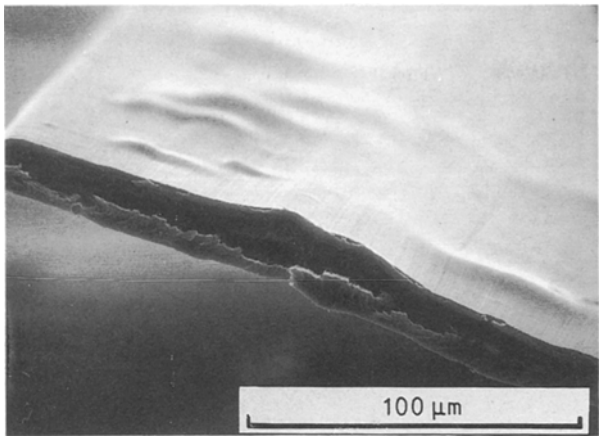

Figure 3 Wrinkled planes in Carbon ribbon cut transversely by a razor blade.

3.1.2. Results and observations

The average longitudinal tensile strength of these ribbons was determined to be 0.6 GPa with a standard deviation of 0.15 GPa. As expected, the average value for the strength was less than the tensile strength of the Pitch-55 fibre of 1.926 GPa [8]. The large reduction in the tensile strength of the ribbons was attributed to the widespread presence of structural inhomogeneities of almost 20 μm size affecting approximately 10–15% of the surface area of the ribbon. The statistical variability in strength of the reference Pitch-55 fibres at a coefficient of variation of 0.22 is primarily governed by imperfections among crystallites, while the larger variability in the ribbons discussed here could be directly assigned to the above mentioned inhomogeneities. The fracture surfaces of the ribbons were surprisingly flat as shown in Fig. 4a in contrast to the zig-zag surfaces that may be expected due to the high variability of axial strength and weak shear strengths across the lamellae. However, some axial delamination during fractures was also recorded as shown in Fig. 4b.

3.2. Measurement of transverse strength of ribbons

Transverse strength of the ribbons was determined by a new laser spallation technique discussed in detail elsewhere [9, 10]. In this technique, a laser pulse of a high enough energy and a pre-determined length is converted into a pressure pulse of a critical amplitude and width that is sent through the thickness direction of the ribbon towards its free surface. The reflected tensile wave from the free surface of the ribbon produces transverse delamination of the ribbon. The critical stress amplitude that accomplishes the internal delamination of the ribbon is determined from a computer simulation of the process. The transverse strengths of the ribbons measured in this manner varied over a wide range of values from 0.13 GPa to 0.26 GPa. This strength level and its large variation were attributed to the structural inhomogeneities shown in Fig. 1 which were present throughout the ribbon. Fig. 5 shows a portion of the ribbon delaminated by this laser spallation technique. It also shows the perturbation in fracture path produced by one of the structural inhomogeneities.

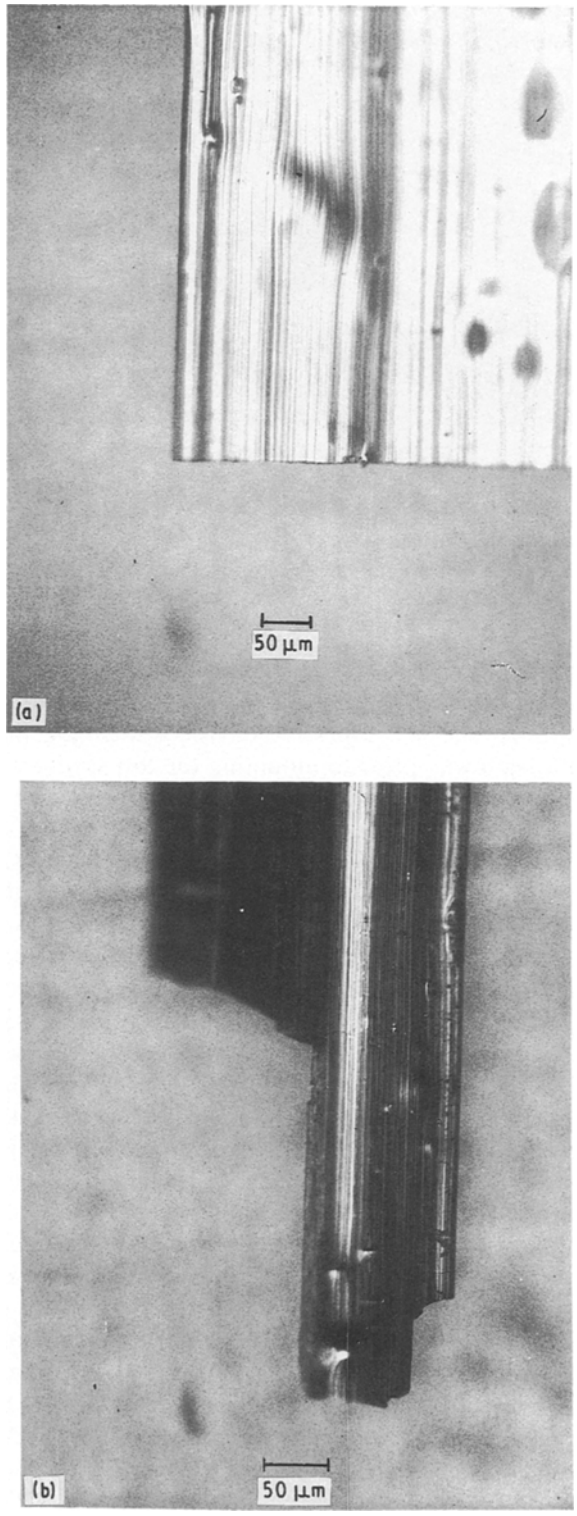

Figure 4 (a) Planar fracture surface typical of most ribbon fractures across the ribbon axis, (b) fracture surface with an axial delamination step, as observed occasionally.

4. Toughness anisotropy of ribbons

4.1. Fracture across the ribbon axis

The determination of the fracture toughness of the ribbons across the ribbon axis required a small but important modification in the test procedure outlined

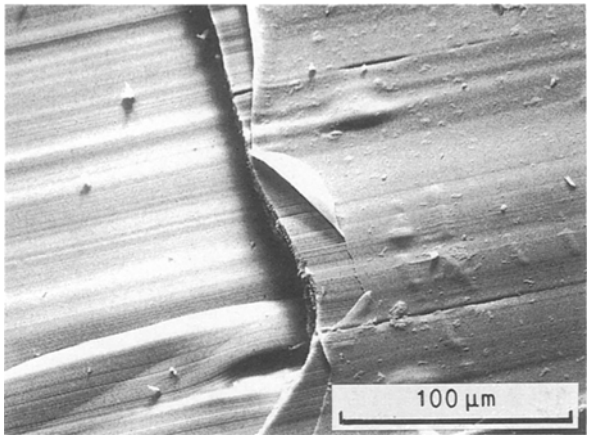

Figure 5 Fracture surface of a Carbon ribbon delaminated in a laser spallation experiment.

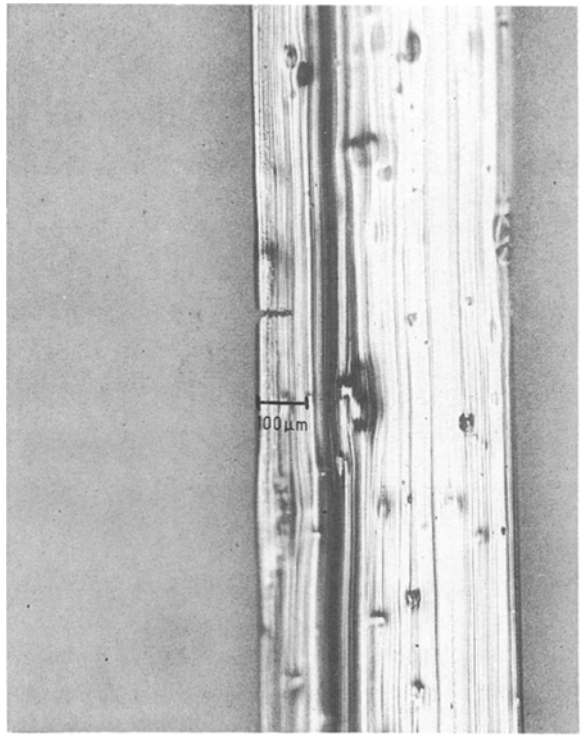

Figure 6 Ribbon showing edge crack cut-in with a razor blade.

in Section 3.1 above. Since pre-cracked ribbons proved to be extremely fragile, and often did not even survive the cutting of the rectangular cardboard test frames on which they were mounted, it was necessary to pre-cut the test frames and then stick them together with bee's wax prior to mounting the test sections of the ribbons on them. With this altered procedure it was then possible to perform the tests readily by mounting the initially intact ribbon segments into the modified test frames, and then carefully notching the secured ribbons on one edge with a sharp razor blade under a stereo light microscope. The initial crack lengths in these edge cracked ribbon strips were then photo-micrographically recorded as shown in the typical case in Fig. 6. The cards bearing the notched ribbons were then inserted into the tension machine, the wax holding together the pre-cut cardboard test frame was melted, and the nominal fracture stress of the freed ribbon was recorded. The fracture toughness K_{Ic} and the energy release rate G_{Ic} were then determined by standard procedures of toughness testing.

Examination of the ribbon fragments showed smooth fracture surfaces and a complete absence of jaggedness indicative of axial delamination during crack propagation, inspite of the expected lower transverse strength of the ribbon. This behaviour will be seen to be fully consistent with the results of the fracture toughness for cracks propagating along the ribbon axis. The average work of fracture G_{Ic} of the ribbons across the graphitic lamellae was determined to be 3.5 $J m^{-2}$ by using the standard formula for K_c for a single edge notched tension specimen.

4.2. Fracture parallel to the ribbon axis

The determination of the work of fracture for cracks propagating parallel to the ribbon axis presented unexpected complexities. The final procedure involving a steady state experiment performed on the microscope stage is shown in Fig. 7. A sharp cleavage knife in the form of a single edge razor blade is attached with an outrigger arm to the objective of a light microscope in a manner to position the cutting edge of the knife well within the field of view of the objective. A test section

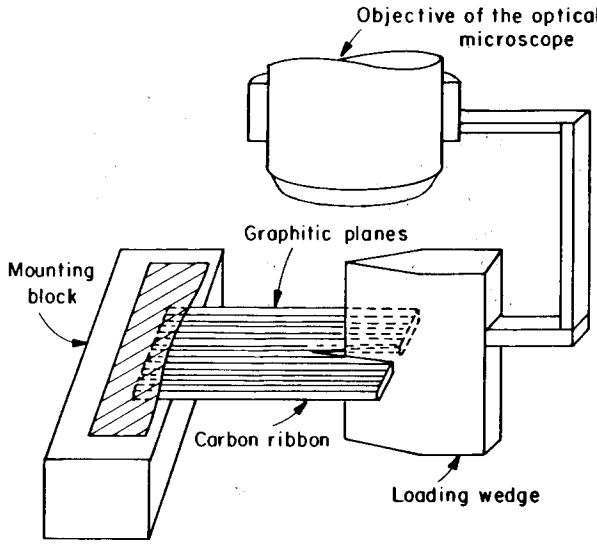

Figure 7 Experimental set-up to measure the delamination fracture work in ribbons for cracks propagating along the ribbon axis.

of a carbon ribbon of 5 mm length was mounted as a cantilever beam on a block that in turn was firmly attached to the horizontal (x) motion of a microscope stage x–y drive, with the axis of the ribbon lying parallel to the x direction of the stage motion. The test was carried out by pushing the ribbon against the knife edge to develop a steady state splitting delamination process. The final determination of the critical stress intensity K_{Ic} or the associated specific fracture work G_{Ic} then required the measurement of the steady state length of the crack between its tip and the points of contact of the edge of the cleavage knife (razor blade). Under ideal conditions the length of the crack could be determined by viewing the ribbon in transmitted light as shown in Fig. 8. The steady state crack

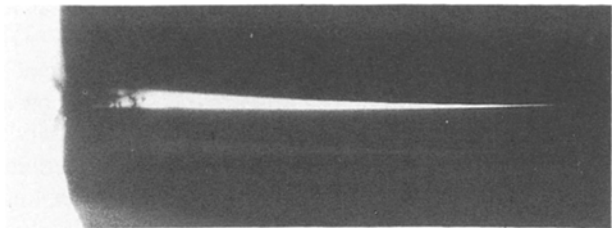

Figure 8 Steady state wedge crack in a ribbon being delaminated by the method shown in Fig. 7, as viewed in a light microscope with transmitted light illumination.

length measured in this manner and the thickness of the razor blade were then sufficient to determine the fracture toughness and G_{Ic}.

Using standard stress intensity factor formulae for the double cantilever beam geometry [7] the plane strain fracture energy release rate G_{Ic} for the ribbon can be written as

$$G_{Ic} = (1 - \nu^2)\frac{PL^2}{EIb} \quad (1)$$

where P, L, I and b are, respectively, the bending force, crack length, moment of inertia of one arm and the width of the ribbon, while E and ν are the Young's modulus and Poisson's ratio of the ribbon, respectively. Using elementary beam theory, Equation 1 can be expressed as

$$G_{Ic} = \frac{3}{16}\left(\frac{\Delta^2}{L^4}\right)Ed^3 \quad (2)$$

where Δ is the critical crack opening displacement (the thickness of the razor blade) and d is the depth of the individual carbon ribbon beam. The values of G_{Ic} calculated from various micrographs using Equation 2 are given in Table I. The axial Young's modulus ($E = 150$ GPa) of the carbon ribbon used in Equation 2 for calculating G_{Ic} was determined independently from the tensile tests on ribbons.

The G_{Ic} values reported in Table I are extremely high when compared with the value of 3.5 J m^{-2} determined for fracture across the ribbon axis. Since the calculated toughness depends sensitively on the steady state cantilever beam length L it was essential to establish that no significant error was made in the experimental measurement of this quantity. A point of particular concern was the possibility of a twist bend-buckling instability in the slender cantilever arms that would both invalidate the analysis leading to Equation 2 and also result in an associated spuriously short length of the wedge shaped bright zone shown in Fig. 8. A check with the classical twist-bend-buckling analysis [11] indicated that the conditions of the experiment were well within the limits of stability of the double cantilever beam. Moreover, a repetition of the experiment in the SEM showed, as can be seen in Fig. 9, that the arms of the cantilever remain flat and that the crack length measured with the SEM is the same as that measured by the light microscope in transmission. The additional toughness measurements made *in-situ* in the SEM are also listed in Table I without an "a". Thus, it was necessary to accept these high toughness values as genuine and attribute them to a crack tip plasticity phenomenon resulting from a specific kinking type of plastic deformation by shear along axial planes parallel to the crack plane, discussed in some detail by Rice [12] for the analogous case of crystal plasticity. It is essential to note parenthetically that such elevations in toughness could not be a result of crack trapping [13] due to the inhomogeneity in the ribbon discussed above. These are too few to produce a significant effect.

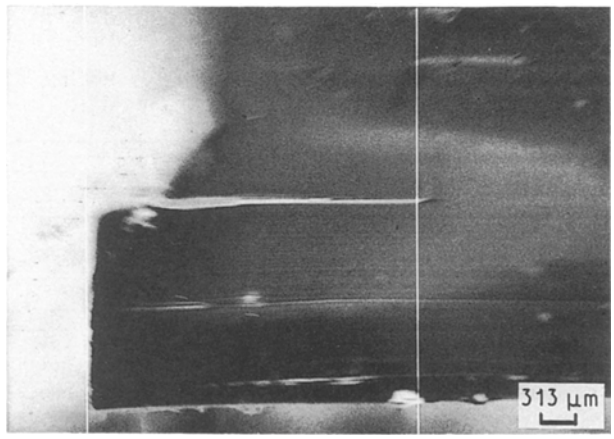

Figure 9 Same experiment as shown in Figs 7 and 8, but performed in an SEM.

TABLE I G_{Ic} values obtained from the microscope stage delamination tests

Sample no.	Depth of beam (m)	Length of beam (m)	CTOD (m)	G_{Ic}[b] from Equation 2 (J/m^2)
1[a]	2.50×10^{-4}	1.74×10^{-3}	6.25×10^{-5}	158
2[a]	1.98×10^{-4}	8.30×10^{-4}	2.17×10^{-5}	183
3	2.64×10^{-4}	3.23×10^{-4}	2.00×10^{-6}	160
4	2.34×10^{-4}	1.38×10^{-3}	4.46×10^{-5}	166
5[a]	2.64×10^{-4}	1.69×10^{-3}	5.28×10^{-5}	150
6[a]	2.86×10^{-4}	3.62×10^{-4}	1.13×10^{-5}	155
7	3.00×10^{-4}	5.24×10^{-4}	5.53×10^{-5}	170
8	2.17×10^{-4}	1.81×10^{-3}	8.7×10^{-5}	171
9	2.38×10^{-4}	1.19×10^{-3}	3.39×10^{-5}	165

[a] Calculated from light micrographs. Others from SEM micrographs.
[b] Axial modulus of the ribbon used to calculate G_{Ic} is 150 GPa.

As is well known in cleavage type fractures with accompanying inelastic dissipation, the plastic dissipation energy G_p is both proportional to the intrinsic work of cleavage G_{co} and additive to it, [14] i.e.

$$G_{Ic} = G_{co} + G_p = G_{co}(1 + K) \quad (3)$$

and

$$K = \frac{G_p}{G_{co}} \quad (4)$$

Evidence for the kinking type of crack tip plasticity is shown in Fig. 10a which is an SEM view of the crack tip in one of the *in-situ* double-cantilever delamination tests. Fig. 10b shows a sketch of the kinking plastic zone ahead of this crack. It appears that much of the kinking displacements are reversible as the crack leaves the kinked zone behind in its wake.

A quantitative accounting for the plastic energy dissipation requires the determination of the interlaminar longitudinal shear resistance of the ribbon material. We discuss the measurement of this shear resistance in Section 4.3 below prior to a discussion in Section 4.4 of the mechanics accounting for the inelastic energy dissipation accompanying the axial delamination of ribbons.

4.3. Interlaminar longitudinal shear resistance

The interlaminar longitudinal shear resistance of ribbons was determined by employing a special torsion experiment as shown in Fig. 11. In this set up the carbon ribbon of 2 cm length (A–B) is mounted in series with a tungsten wire torsion spring (C–D), having a well known spring constant, on the frame of a vertical metallograph. The upper part of the ribbon is effectively fixed to the frame of the metallograph while the lower part is attached to a small intermediate metal platelet (C) which also carries a pointer and clamps the upper part of the tungsten torsion spring. The pointer attached to the metal platelet, permits the measurement of the total twist angle in the ribbon. The lower part of the tungsten wire torsion spring is attached to the centre of the rotary goniometer stage of the metallograph.

The elastic-plastic torque-twist response of the ribbon is obtained by monotonically rotating the lower goniometer stage of the microscope and simultaneously recording the angles of rotation of the lower stage and the pointer mounted on the intermediate

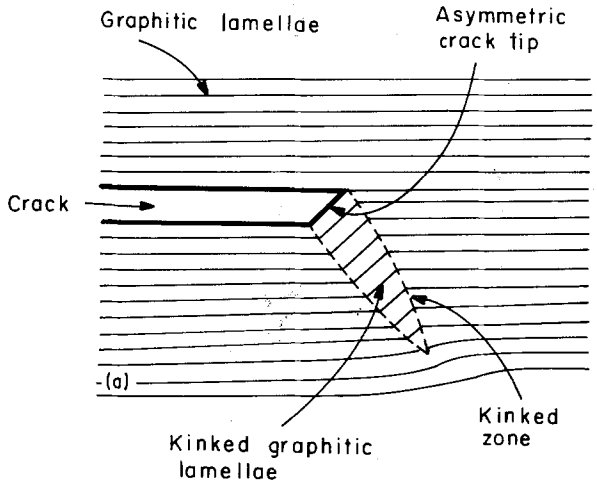

Figure 10 (a) Sketch of the kinking displacements at a crack tip; (b) high magnification micrograph showing a delamination crack blunted by a crack tip kinking type plastic zone.

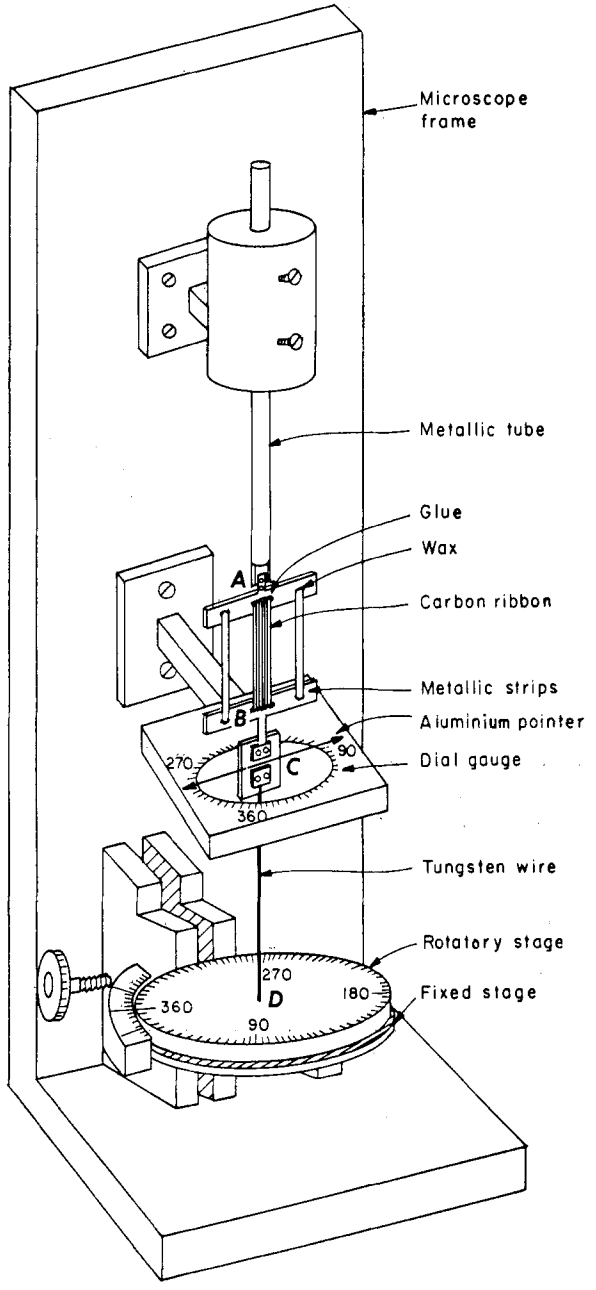

Figure 11 Schematic view of the torsion experiment to measure inelastic properties of the ribbon.

metal platelet. While the difference in angles of rotation θ_D and θ_C, together with the torsional stiffness of the tungsten wire, gives the total twisting moment M in the assembly, the angle θ_C becomes the total twist in the ribbon.

Thus

$$M = (\theta_D - \theta_C)\frac{J_w \mu_w}{L_w} \quad (5)$$

where J_w, μ_w, and L_w are respectively the torsional moment of inertia, the shear modulus and the length (C–D) of the tungsten wire torsion spring. In the early phases of the test while the behaviour of the carbon ribbon is still linearly elastic, we also have

$$M = \frac{\theta_c J_r \mu_r}{L_r} \quad (6)$$

where J_r, μ_r, and L_r are, respectively, the torsional moment of inertia, the effective axial shear modulus and the length of the carbon ribbon. Upon yielding of the ribbon by longitudinal shear the angle of twist θ_C and M no longer remain linearly proportional as given in Equation 6. A typical plot of $\theta_D - \theta_C$ against θ_C is shown in Fig. 12, where point S in the figure shows where the ribbon first undergoes plastic deformation by longitudinal shear, at a critical torque M_c. For a ribbon of width b and thickness t the critical resolved shear stress τ_y for longitudinal shear is then [11].

$$\tau_y = \frac{3M_c}{bt^2} \quad (7)$$

From the curve in Fig. 12 it is found that $\tau_y = 83$ MPa. The relevant dimensions and material constants used in calculating the value τ_y are given in Table II. The effective shear modulus μ_r of the ribbon can be calculated from Equation 6 by using the slope $dM/d\theta_C$ of the curve. This gave $\mu_r = 65$ GPa. Another independent measure of the shear modulus was obtained from a torsional vibration test utilizing a segment of a ribbon of length l as a torsional spring and a simple cylindrical "flywheel" mass m of radius R attached to the end of the ribbon. The effective longitudinal shear modulus μ_r can then be determined from the measured natural frequency f of the system and is

$$\mu_r = 6\pi^2 \frac{mR^2 l f^2}{bt^3} \quad (8)$$

The average shear modulus obtained in this manner was 51 GPa. Although the value of τ_y appears high, it is only 0.16% of the shear modulus. Thus, with such a comparatively low shear resistance plastic flow by longitudinal shear should occur readily in the kinking mode discussed above, when axial cracks propagate along the length of the ribbon.

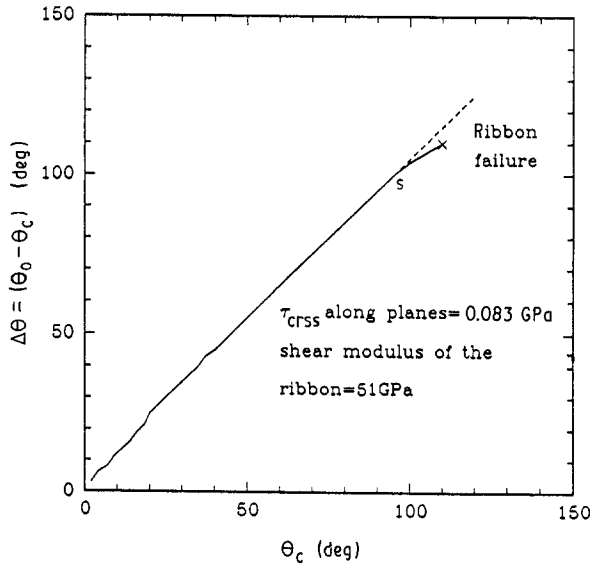

Figure 12 Plot of $\Delta\theta$ against θ_C as recorded in the torsion experiment.

4.4. Plastic dissipation during axial delamination of ribbons

An estimate of the plastic work that accompanies axial delamination was obtained by employing the asymptotic elastic-plastic stress analysis of Rice [12] for a crack in single crystals undergoing plasticity by slip. This analysis which permits the incorporation of plastic anisotropy in determining the asymptotic structure of the crack tip stress and deformation fields was applied here to the cracks growing in the carbon ribbon. The dissipative plastic work during the crack propagation was estimated by integrating the product of the accumulated plastic strain with the shear stress along the elastic/plastic boundary over the total crack advance.

In this analysis, the details of which can be found elsewhere [15], it is recognized that the carbon ribbon has a fibre texture, i.e., the precursor chain molecules are aligned along the ribbon axis, treated here as the c axis of a hexagonal crystal. Thus, when a crack propagates along the c axis, the crack plane can be taken to be on any prism plane with its tip lying parallel to any direction in the base plane. Because of the chain slip nature of the plastic shear, the shear resistance τ_o ($= \tau_y$) must be lowest on prism planes along the c direction. Thus, as already stated, the carbon ribbon can be approximated as an aggregate of hexagonal crystals with their c axes parallel to the ribbon axis but with their hexagonal a, b axes being randomly oriented perpendicular to the ribbon axis. Based on the above geometrical model, the method of

TABLE II Relevant geometrical and material parameters for the Carbon ribbon and Tungsten wire used in torque–twist behaviour determination

	Ribbon	Tungsten wire
Shear Modulus μ, (GPa)	51[a]	170
Young's Modulus, E (GPa)	150	411
Length, L (m)	7.93×10^{-3}	61.0×10^{-3}
Torsional moment of inertia, J, (m^4)	9.28×10^{-18}	1.28×10^{-17}
Thickness, t (m)	35.0×10^{-6}	—
Radius, r (m)	—	6.35×10^{-5}
Width, b (m)	6.50×10^{-4}	—

[a] Determined from the torsional vibration test.

Rice [12] then was applied to determine the crack-tip stresses for the case when the crack is on the $(01\bar{1}0)$ plane and its tip lies along the $[2\bar{1}\bar{1}0]$ direction of the reference hexagonal crystal, so that $[0001]$ is the direction of the crack growth parallel to the ribbon axis. The high crack-tip stresses are predominantly relieved by prismatic slip on the $(01\bar{1}0)$ plane along the $[0001]$ direction in the kinking mode. In the reference hexagonal crystal other slip systems that intersect the crack plane and help to accommodate the stresses are: pyramidal slip systems consisting of simultaneous slips on $(01\bar{1}1)$ planes along the $[1\,1\,\bar{2}\,\bar{3}]$ and $[\bar{1}2\bar{1}\bar{3}]$ directions, and simultaneous slips on the $(0\bar{1}11)$ plane along the $[1\bar{2}1\bar{3}]$ and $[\bar{1}\bar{1}2\bar{3}]$ directions. In the ribbon morphology, however, there are no specific analogs to these slip systems, so they were not considered. Total plastic work dissipated as the crack grows is then due to the accumulation of the plastic strain of the type $\gamma^{p}_{r\theta}$ (albeit in the kinking mode) at the elastic/plastic sector boundary. Due to the extremely small range of the wake region 0.82°, the plastic work accumulated inside the wake region is very small, hence, the contribution of it to the total dissipated work can be neglected. The plastic work was then calculated by integrating the product of the accumulated plastic strain with the shear stress along the elastic/plastic boundary over the total crack advance as

$$G_p = 2\int_0^{r_p} \sigma_{r\theta}\gamma^{p}_{r\theta}\,dr = 2\tau_y\int_0^{r_p}\gamma^{p}_{r\theta}\,dr \quad (9)$$

where $\sigma_{r\theta}$ was equated to τ_y, the measurement of which was discussed in Section 4.3 above. Using the expression for the accumulated plastic strain derived in [15], we obtain the following expression for the plastic work dissipated per unit area of crack advance

$$G_p = 0.97\frac{(K_{Ic})^2}{E}(1-\nu^2) = 0.97\,G_{Ic} \quad (10)$$

where K_{Ic} is the effective fracture toughness that results in the delamination.

The plastic work of axial delamination as calculated from Equation 10 using the experimental values of K_{Ic} from Table I are given in Table III. Equation 10 indicates that approximately 97% of the total fracture energy, G_{Ic}, is dissipated when deforming the material inelastically by the kinking mode.

As indicated by Equation 3, the remaining energy is the intrinsic axial "cleavage" work for the ribbon material. These calculated numbers given in Table III are well within the expected typical intrinsic toughness values of ca. 5 J m^{-2}. Thus, it is possible to account, at least broadly, for the experimentally observed high toughness values using the analysis technique of Rice [12].

TABLE III Estimation of intrinsic toughness values

G_{Ic} values from Table I (J m^{-2})	G_p values (J m^{-2}) Calculated from Equation 10	Intrinsic toughness values as estimated using Equation 3
158	153.3	4.7
183	177.5	5.5
160	155.2	4.8
166	161.0	5.0
150	145.5	4.5
155	149.3	4.7
170	164.9	5.1
171	165.9	5.1

Parenthetically, these high axial delamination toughnesses also are in support of the remarkably flat fracture surfaces for cracks propagating normal to the ribbon axis. Thus any departure of the transverse crack into the axial direction should be effectively stifled.

5. Discussion

Achieving the goals of a strategy of deflecting cracks in a controlled manner along interfaces in composites require also the experimental determination of the strength and toughness of the reinforcing fibres to assess the likelihood of alternative crack paths. How these considerations enter the specific delamination criteria has been discussed by Gupta *et al.* [4]. Since such measurements are difficult to make in fibres that are often 10 μm in diameter or even smaller, specially prepared Pitch-55 ribbons of 600 μm width and 35 μm thickness were used for these tests. As in the case of carbon fibres, the ribbons showed strong elastic anisotropy. Hence, the strengths and fracture energies along and across the graphitic planes were determined. The average longitudinal tensile strength for fracture across the ribbon axis was determined to be 0.6 GPa. This value is considerably lower than that for the fibre (1.93 GPa). This strength reduction is attributed to structural inhomogeneities in the ribbon distributed throughout the volume. The transverse strength values varying from 0.13 GPa to 0.26 GPa were obtained from a laser spallation experiment. Here too the low values of the transverse strength and the associated large scatter is attributed to the distribution of structural inhomogeneities within the ribbon material.

The average fracture energy for fracture across the ribbon axis, measured by standard fracture mechanics tests performed on single edge cracked ribbons was determined to be 3.5 J m^{-2}.

Unusually high work of fracture values of 166 J m^{-2} were obtained for cracks propagating along the graphitic lamellae. These high values result from a relatively profuse kinking type of crack tip plasticity on the graphitic lamellae lying by shear parallel to the crack plane. An asymptotic elastic-plastic analysis for the cleaving of single crystals, as formulated by Rice [12], was adopted to estimate the extent of inelastic energy dissipation. These estimates gave results that could account for the experimentally observed high values of plastic dissipation and were compatible with intrinsic toughness values in the range of 5 J m^{-2} (Equation 3). Thus, the stresses in the vicinity of the crack tip running in the axial direction are relieved predominantly by the relaxation of the shear stresses acting across the graphitic lamellae lying parallel to the crack plane. In a material having low interlaminar shear strength, crack tip plasticity can be expected to

be entirely of a kinking type shown in Fig. 10a. Evidence for this is presented in Fig. 10b. The calculations for the inelastic energy dissipation require information on the interlaminar shear resistance across the graphitic lamellae. This information was obtained by a special torsion test leading to a shear resistance of 83 MPa, and also to an in-plane longitudinal shear modulus of 65 GPa. A separate measurement of this shear modulus was also obtained from a torsional vibration test and was found to be 51 GPa.

Acknowledgement

This research was supported by the Office of Naval Research under contract N00014-85-K-0645. For this support we are grateful to Dr. S. Fishman of that agency. We are also grateful to Dr. E. M. Schultz of the DuPont company who furnished the Pitch-55 carbon ribbons that made this investigation possible.

References

1. A. S. ARGON, in "Treatise on materials science and technology", Vol. 1, edited by H. Herman (Academic Press, New York, 1972), p. 79.
2. *Idem*, in "Composite materials: fracture and fatigue", Vol. 5, edited by L. J. Broutman and R. H. Krock (Academic Press, New York, 1974), p. 153.
3. V. GUPTA, A. S. ARGON and J. A. CORNIE, *J. Mater. Sci.* **24** (1989) 2031.
4. V. GUPTA, Z. SUO and A. S. ARGON, *J. Appl. Mech.* in press.
5. A. S. ARGON, V. GUPTA, H. S. LANDIS and J. A. CORNIE, *J. Mater. Sci.* **24** (1989) 1207.
6. R. BACON, in Proceedings of a conference on metal and ceramic matrix composites processing (U.S. Department of Defense, Columbus, Ohio, 1984) (limited circulation) Vol. 2, p. 23.
7. H. P. TADA, P. C. PARIS and G. R. IRWIN, The stress analysis of cracks hand-book (Del Research Publication, Hellerton, PA, 1973).
8. Q. LI, in "Strength and fracture behaviour of SiC coated graphite fibres in the characterization of interfaces in Carbon fibre-Aluminum matrix composites", S. M. Thesis, Department of Materials Science and Engineering, (M.I.T., Cambridge, MA, 1988).
9. V. GUPTA, A. S. ARGON, D. M. PARKS and J. A. CORNIE, *Mater. Sci. and Engng* **A126** (1990) 105.
10. *Idem, J. Mech. Phys. Solids*, in press.
11. H. P. DEN HARTOG, in "Advanced strength of materials" (McGraw-Hill, New York, 1952).
12. J. R. RICE, *Mech. Mater.* **6** (1987) 317.
13. B. BUDIANSKY, J. W. HUTCHINSON and A. G. EVANS, *J. Mech. Phys. Solids*, **34** (1986) 167.
14. J. R. RICE, in Proceedings of the First International Conference Fracture, edited by T. Yokobori, T. Kawasaki and J. L. Swedlow (The Japanese Society for Strength and Fracture of Materials, Sendai, Japan, 1966) Vol. 1, p. 309.
15. V. GUPTA, Ph.D. Thesis, Department of Mechanical Engineering (M.I.T., Cambridge, MA, 1990).

Received 9 October 1990
and accepted 24 January 1991